Liquid Crystals, Vol. 33, No. 7, July 2006, 811–818

Taylor & Francis
Taylor & Francis Group

Ionic interaction induced novel ordered columnar mesophases in asymmetric discotic triphenylene salts

LI CUI and LEI ZHU*

Polymer Program, Institute of Materials Science and Department of Chemical Engineering, University of Connecticut, Storrs, Connecticut 06269-3136, USA

(*Received 19 January 2006; accepted 11 April 2006*)

Asymmetric triphenylene imidazolium salts with different spacer lengths were successfully synthesized through quarternization of ω-bromo-substituted triphenylenes with 1-methyl imidazole. The asymmetry in ω-bromo-substituted triphenylenes tended to destroy liquid crystallinity in the sample. However, highly ordered columnar mesophases with a lamellar microphase segregation were induced by ionic interactions among the imidazolium salts, and the lamellar morphology was visualized by transmission electron microscopy. On the basis of an X-ray diffraction study on shear oriented samples, a novel rectangular columnar phase with a plane group of *pm* was observed for a triphenylene imidazolium salt with a spacer length of C_{11}, while an oblique columnar phase was determined for a triphenylene imidazolium salt with a C_8 spacer. Due to the asymmetric molecular shape and ionic interactions in the triphenylene imidazolium salts, the columnar liquid crystalline phase was extended to below room temperature (*c.* -20°C) for samples with spacer lengths of C_8 and C_{11}.

1. Introduction

Having a high charge-mobility in their columnar mesophases, discotic liquid crystals (LCs) are excellent candidates for charge transport in organic microelectronics and photonics [1]. However, for practical applications, a wide liquid crystalline temperature range with a lower limit below room temperature is generally desired. Hexa-*peri*-hexabenzocoronene (HBC) based discotic LCs were reported to exhibit a wide columnar liquid crystalline range from slightly below room temperature to $>400^{\circ}$C [2]. To avoid the complicated synthesis of HBC, simpler molecules such as triphenylenes have also been investigated, and a few systems exhibited broad liquid crystalline ranges down to room temperature [3].

In addition to low temperature liquid crystalline transitions, mesophase self-assembly in discotic molecules has also attracted much attention. In general, mesogen shape and specific intermolecular interactions such as hydrogen bonding and ionic interactions dictated the supramolecular assembly of discotic LCs. For example, layer structures rather than two-dimensional (2D) columnar phases were recently observed in combined discotic and calamitic molecules, where molecular architecture and topology played an important role [4]. These low-order layer structures were different from highly ordered lamello-columnar (Col_L) phases previously reported [5]. Meanwhile, ionic interactions were found to stabilize columnar liquid crystalline self-assembly in triphenylene imidazolium salts [3(*c*), 6]. For symmetric (hexa-substituted) triphenylene imidazolium salts, the hexagonal columnar phase existed over a wide temperature range [3*c*]. Although asymmetric (mono-substituted via an ether linkage) triphenylene imidazolium salts have recently been synthesized [6], no details on their phase structure and morphology have yet been reported.

In this work, we synthesized asymmetric (mono-substituted via an ester linkage) triphenylene imidazolium salts with various spacer lengths (C_5, C_8, and C_{11}) to study the effect of spacer length on their supramolecular assembly and phase morphology (see scheme 1). On the basis of X-ray diffraction (XRD) experiments, novel columnar mesophases with a high degree of layer ordering were induced by ionic interactions in the asymmetric imidazolium salts. For example, because of the asymmetry in compound **2c**, a new rectangular columnar (Col_r) symmetry, *pm*, instead of the recently reported simple Col_r symmetry, *p2mm* (or *P2m*) [7], was observed for the first time. Meanwhile, the columnar liquid crystalline phase in **2c** persisted down to its glass transition temperature (T_g) at -20°C, which might lead to potential applications at room temperature.

*Corresponding author. Email: lei.zhu@uconn.edu

Liquid Crystals
ISSN 0267-8292 print/ISSN 1366-5855 online © 2006 Taylor & Francis
http://www.tandf.co.uk/journals
DOI: 10.1080/02678290600791986

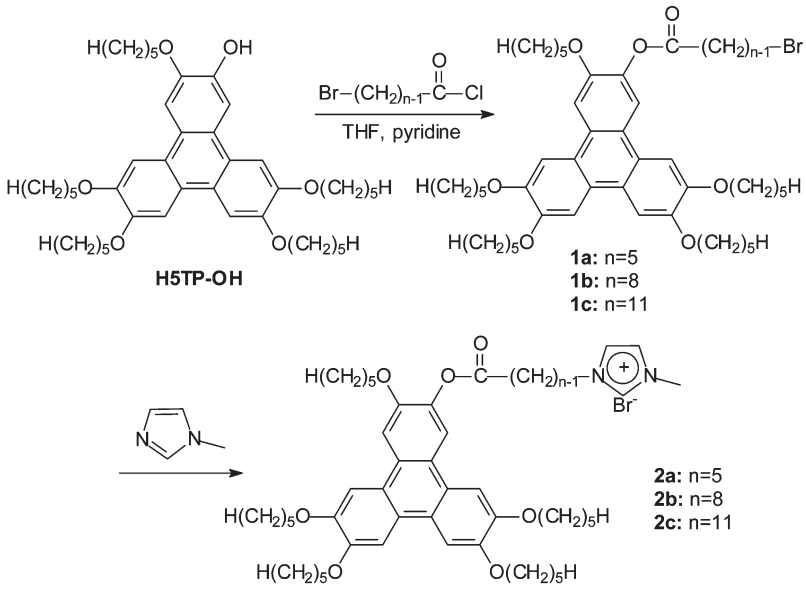

Scheme 1. Synthesis of triphenylene imidazolium salts **2a**–**c** with different spacer lengths.

2. Experimental

2.1. *Synthesis*

Triphenylene imidazolium salts **2a**–**c** were synthesized by quaternization of ω-bromo-substituted triphenylenes (**1a**–**c**) with 1-methylimidazole (scheme 1). Detailed synthesis and molecular characterization by ^{1}H NMR, mass spectroscopy (MS), and chromatography have been described in a separate report [8]. Briefly, 2-hydroxy-3,6,7,10,11-pentakis(pentyloxy)triphenylene (P5T-OH) was prepared by cleavage of 2,3,6,7,10, 11-hexakis(pentyloxy)triphenylene [9(*a*, *b*)] with 1.2 equivalents of B-bromocatecholborane [9(*c*)]. ω-Bromo-substituted triphenylenes **1a**–**c** were prepared by esterification via reactions of P5T-OH with ω-bromoacyl chloride. Quaternization of **1a**–**c** with 1-methylimidazole afforded the asymmetric triphenylene imidazolium salts **2a**–**c**. The final products were purified by flash column chromatography and their identity confirmed by ^{1}H NMR and MS.

2a was obtained as a brown solid in a yield of 70%. ^{1}H NMR (δ, $CDCl_3$): 0.98 (t, J 7.2 Hz, CH_3, 15H) 1.44–1.56 (m, $CH_3C\underline{H}_2C\underline{H}_2$, 20H), 1.62–1.97 (m, $C\underline{H}_2CH_2O$, $C\underline{H}_2CH_2COO$, $C\underline{H}_2CH_2$–N^+, 14H), 2.74 (t, J 6.4 Hz, CH_2COO, 2H), 3.79 (s, CH_3–N, 3H), 4.24 (m, CH_2O, 10H), 4.48 (s, CH_2–N^+,2H), 7.03–7.13 (m, Im–H, 2H), 7.7–8.1 (m, Ar–H, 6H), 11.27 (s, Im–H, 1H). MS (electrospray ionization, ESI): 839.4 (100%, this mass was consistent with the fragment without Br^- anion, $C_{52}H_{75}N_2O_7$, 840.18), 769.4 (4%), 281.9 (5%), 196.9 (8%).

2b was obtained as a brown and wax-like solid in a yield of 56%. ^{1}H NMR (δ, $CDCl_3$): 0.99 (t, J 7.1 Hz, CH_3, 15H) 1.34–1.59 [m, $CH_3C\underline{H}_2C\underline{H}_2$ and $(C\underline{H}_2)_3CH_2CH_2$–$N^+$, 26H], 1.87 (m, $C\underline{H}_2CH_2COO$, 2H), 1.96 (m, $C\underline{H}_2CH_2$–N^+ and $C\underline{H}_2CH_2O$, 12H), 2.69 (t, J 6.5 Hz, CH_2COO, 2H), 3.76 (s, CH_3–N, 3H), 4.24 (m, CH_2O, 10H), 4.44 (s, CH_2–N^+,2H), 7.10–7.18 (m, Im–H, 2H), 7.7–8.1 (m, Ar–H, 6H), 10.96 (s, Im–H, 1H). MS (ESI): 881.4 (100%, this mass was consistent with the fragment without Br^- anion, $C_{55}H_{81}N_2O_7$, 882.26), 550.5 (6%), 509.2 (13%), 240.0 (42%), 238.7 (100%), 224.8 (25%), 194.1 (11%), 82.9 (28%).

2c was obtained as a yellow and soft solid in a yield of 65%. ^{1}H NMR (δ, $CDCl_3$): 0.99 (t, J 6.9 Hz, CH_3, 15H) 1.35–1.57 [m, $CH_3C\underline{H}_2C\underline{H}_2$ and $(C\underline{H}_2)_6CH_2CH_2$–$N^+$, 32H], 1.88 (m, $C\underline{H}_2CH_2COO$, 2H), 1.97 (m, $C\underline{H}_2CH_2$–N^+ and $C\underline{H}_2CH_2O$, 12H), 2.69 (t, J 6.8 Hz, CH_2COO, 2H), 4.0 (s, CH_3–N, 3H), 4.24 (m, CH_2O and CH_2–N^+, 12H), 6.98 (s, Im–H, 1H), 7.07 (s, Im–H, 1H), 7.7–8.1 (m, Ar–H, 6H), 10.75 (s, Im–H, 1H). MS (ESI): 923.4 (100%, this mass was consistent with the fragment without Br^- anion, $C_{58}H_{87}N_2O_7$, 923.34), 282 (12%), 279.9 (61%), 266.9 (4%), 73.9 (4%).

2.2. *Characterization*

^{1}H NMR spectra were recorded at 293 K in $CDCl_3$ on a Bruker spectrometer (500 MHz, DMX 500), with tetramethylsilane as the internal reference. The MS spectra were performed on a Micromass Quattro II with an ESI at a cone voltage of 30 V. Differential scanning calorimetry (DSC) was carried out on a TA Q-100 DSC

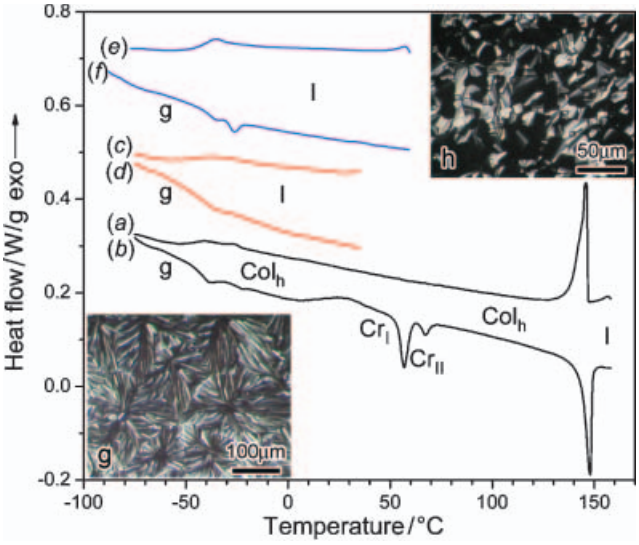

Figure 1. DSC curves of **1a** [(a) first cooling, (b) second heating], **1b** [(c) first cooling, (d) second heating], **1c** [(e) first cooling, (f) second heating]. Insets (g) and (h) show POM micrographs for the crystalline and Col$_h$ phases of **1a**.

instrument; an indium standard was used to calibrate the instrument. Approximately, 3 mg of sample was used for the DSC study and the scanning rate was 5°C min^{-1}. Wide angle X-ray diffraction (WAXD) was performed using a tube X-ray operating at 1.6 kW with the CrK$_\alpha$ radiation (wavelength λ=0.229 nm). Two-dimensional (2D) data were recorded using a Bruker AXS area detector with a general area detector diffraction system (GADDS). Polarizing optical microscopy (POM) experiments were performed using an Olympus BX51P microscope equipped with an Instec HCS410 hot stage. Transmission electron microscopy (TEM) experiments were performed on a Philips EM300 at an accelerating voltage of 80 kV. Thin sections of thickness *ca.* 70 nm were obtained using a Leica Ultracut UCT microtome equipped with a diamond knife at −40°C. The thin sections were collected onto 400 mesh copper grids, freeze-dried, and stained by I_2 vapour at room temperature for 6 h [10].

3. Results and discussion

3.1. *Thermal and phase behaviour of asymmetric triphenylenes 1a–c*

The phase transitions of asymmetric triphenylenes **1a**–**c** were studied by DSC and their phase structures were identified by POM. As seen in figure 1, upon cooling, the isotropic (I) to hexagonal columnar phase (Col$_h$) transition for **1a** was at 146°C. The glass transition temperature (T_g) was at −46°C. Upon heating it had a T_g of −45°C, a cold-crystallization peak at 29°C, a crystal (Cr$_I$) melting peak at 57°C, a Cr$_{II}$ to Col$_h$ transition at 67°C, and finally a peak isotropization temperature (T_I) at 148°C. Representative POM micrographs of the crystalline and Col$_h$ phases for **1a** are shown in the insets (g) and (h) of figure 1, respectively. **1b** had only a T_g at −45°C; **1c** had a T_g at −41°C and a small crystal melting at −26°C during heating. Therefore, no LC phases were observed in asymmetric **1b** and **1c** for a spacer length ⩾C$_8$. This result is somewhat different from a recent report for asymmetric triphenylenes with five of the same OC$_6$H$_{13}$ arms and one different OC$_n$H$_{2n+1}$ arm (n=2–14, 16 and 18) [11]. In that report, Col$_h$ phases were observed for asymmetric triphenylenes with one arm smaller than twice the length of the other arms (i.e. $n \leqslant 12$), while no liquid crystallinity was observed for compounds with $n \geqslant 13$. We speculate that the ω-bromo-substitution and an ester linkage in the triphenylene molecules may be responsible for this difference. However, when **1b** and **1c** were stored at room temperature for a long time, they could crystallize with melting temperatures of ~45°C for **1b** and ~37°C for **1c**, as determined by POM. The thermal behaviour of **1a**–**c** are summarized in table 1.

Table 1. Summary of phase transition temperatures (°C, above the arrow) and heat of fusion (kJ mol^{-1}, below the arrow) for asymmetric triphenylenes **1a**–**c**. Cr=crystals; g=glass; Col$_h$=hexagonal columnar; I=isotropic.

Compound	1st cooling	2nd heating
1a	I $\xrightarrow[12.5]{146}$ Col$_h$ $\xrightarrow[0.08\ \text{kJ mol}^{-1}\ \text{K}^{-1}]{-46}$ g	g $\xrightarrow[0.08\ \text{kJ mol}^{-1}\ \text{K}^{-1}]{-45}$ Col$_h$ $\xrightarrow[-5.0]{29}$ Cr$_I$ $\xrightarrow[4.8]{57}$ Cr$_{II}$ $\xrightarrow[0.8]{67}$ Col$_h$ $\xrightarrow[10.5]{148}$ I
1b	I $\xrightarrow[0.10\ \text{kJ mol}^{-1}\ \text{K}^{-1}]{-44}$ g	g $\xrightarrow[0.64\ \text{kJ mol}^{-1}\ \text{K}^{-1}]{-45}$ I
1c	I $\xrightarrow[0.22\ \text{kJ mol}^{-1}\ \text{K}^{-1}]{-43}$ g	g $\xrightarrow[0.36\ \text{kJ mol}^{-1}\ \text{K}^{-1}]{-41}$ Cr $\xrightarrow[1.1]{-26}$ I

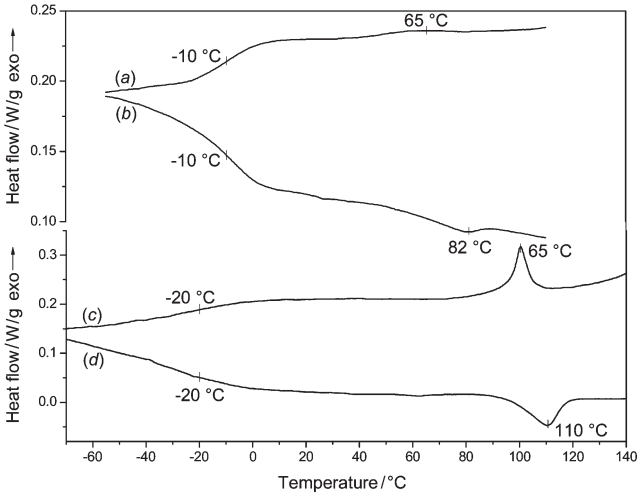

Figure 2. DSC thermograms for **2b** during (*a*) first cooling, (*b*) second heating; **2c** during (*c*) first cooling, (*d*) second heating.

3.2. *Thermal and phase behaviour of asymmetric triphenylene imidazolium salts 2a–c*

The phase transitions in **2a**–**c** were studied by DSC and POM. Compound **2a** was crystalline, and exhibited no liquid crystalline phase behaviour. DSC thermograms for **2b** and **2c** are shown in figure 2. During second heating, **2b** had a T_g at −10°C and a T_I at 82°C; **2c** has a T_g at −20°C and a T_I at 110°C. Between the T_g and T_I, both samples exhibited columnar liquid crystalline phases, which are demonstrated in the POM micrographs in figure 3. The heat of transition for **2b** (1.0 kJ mol^{-1}) was much smaller than that for **2c** (5.1 kJ mol^{-1}). The thermal behaviours of **2a**–**c** are summarized in table 2.

The detailed structure of **2c** was studied by 2D XRD experiments on shear-oriented samples, with the results shown in figure 4. The shear direction was defined as the *x*-direction and the vorticity direction was the *z*-direction. Figure 4A shows the small angle XRD pattern, while figure 4B is the wide angle XRD pattern. When the incident X-ray beam was along the *x*-direction, 2D Col$_r$ columnar structures were identified with the assigned Miller indices shown in figure 4A. The intra-columnar (or face-to-face inter-disk) spacing of 0.35 nm is seen in figure 4B, suggesting an ordered columnar phase. Since this reflection (0.35 nm) was orthogonal to the (0 3) (or layer) reflection (see figure 4B), it was inferred that the normal of the triphenylene disk was oriented parallel to the column axes. We noted that mixed Col$_r$ structures co-existed in the sample, and their schematics are shown in figure 5. Due to the asymmetric shape of the **2c** molecule, both bilayer (figure 5A) and single-layer (figure 5B) structures could form. A fundamental feature in these Col$_r$ phases is the segregation between the aromatic triphenylene and imidazolium groups to form lamellar structures. In figure 4A, the Miller indices for the bilayer Col$_r$ phases are in parentheses and those for the single-layer Col$_r$ phase are in brackets. The unit cell dimensions were determined: (1) for the bilayer Col$_r$ phase, a_1=1.87 nm, b_1=5.25 nm; (2) for the single-layer Col$_r$ phase, a_2=3.38 nm, b_2=3.41 nm. There were two molecules in each unit cell, and hence the density (ρ) for these two phases was ρ_1=0.97 g cm^{-3} and ρ_2=0.83 g cm^{-3} for the bilayer Col$_r$ and single-layer Col$_r$ phases, respectively. Since the XRD intensities

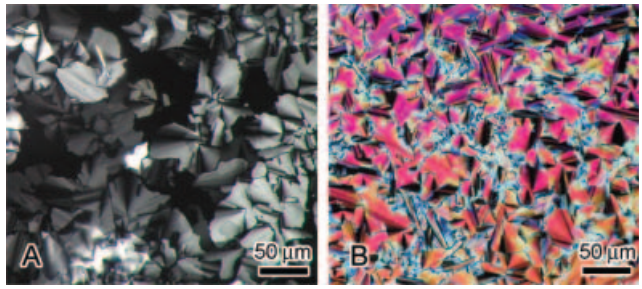

Figure 3. POM micrographs of (A) **2b** at 96°C and (B) **2c** at 95°C.

Table 2. Summary of phase transition temperatures (°C, above the arrow) and heat of fusion (kJ mol^{-1}, below the arrow) for triphenylene imidazolium salts **2a**–**c**. Cr=crystals; g=glass; Col$_o$=oblique columnar; Col$_r$=rectangular columnar; I=isotropic.

Compound	1st cooling	2nd heating
2a	$I \xrightarrow[12.7]{55} Cr_{II} \xrightarrow[8.5]{47} Cr_I$	$Cr \xrightarrow[21.5]{71} I$
2b	$I \xrightarrow[1.0]{65} Col_o \xrightarrow[0.22\ kJ\ mol^{-1}\ K^{-1}]{-10} g$	$g \xrightarrow[0.55\ kJ\ mol^{-1}\ K^{-1}]{-10} Col_o \xrightarrow[1.0]{82} I$
2c	$I \xrightarrow[4.4]{100} Col_r \xrightarrow[0.21\ kJ\ mol^{-1}\ K^{-1}]{-20} g$	$g \xrightarrow[0.21\ kJ\ mol^{-1}\ K^{-1}]{-20} Col_r \xrightarrow[5.1]{110} I$

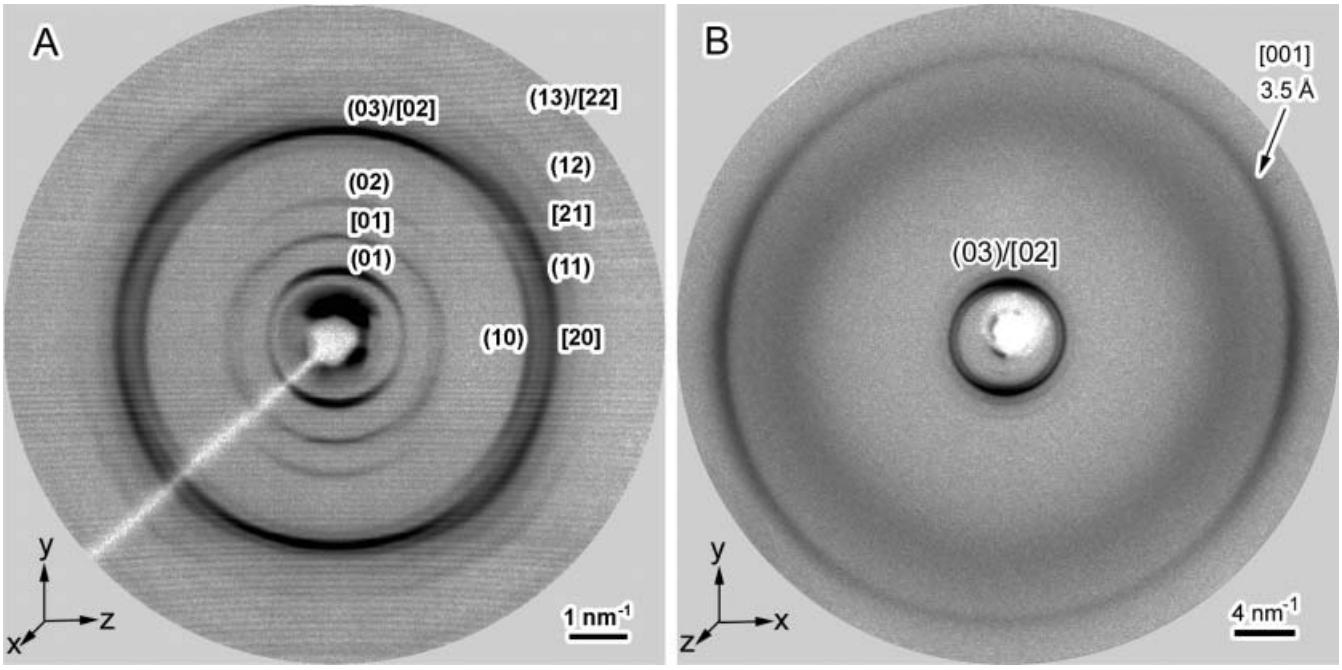

Figure 4. 2D XRD patterns for a shear-oriented **2c** sample in different angular regions: (A) a low angle region with the X-ray along the *x*-direction, (B) a wide angle region with the X-ray along the *z*-direction. Intensities are in logarithm scales.

from the single-layer Col_L phase were lower than those from the bilayer Col_r phase, the bilayer Col_r phase is a major component in the sample.

The bilayer Col_r phase belongs to a new rectangular symmetry, *pm* [12], instead of the conventional *p2gg* (or $P2_1/a$, 2 molecules/cell), *p2mg* (or *P2*/*a*, 4 molecules/cell), *cm* (or *C2*/*m*, 2 molecules/cell) [13], and recently observed *p2mm* (or *P2m*, 1 molecule/cell) and *c2mm* (2 molecules/cell) [7]. No reflection condition is necessary for the *pm* symmetry [12]. The single-layer Col_r phase has a symmetry of *p2mg* (or *P2*/*a*). Different from the conventional *p2mg* phase, it has only 2 molecules per unit cell. The reflection condition is $h\,0$ when $h=2n$ [12].

The existence of mixed structures in **2c** was further confirmed by the observation of double T_I values in the first heating in DSC (see figure 6). It was deconvoluted into two peaks centred at 117°C (2.7 kJ mol^{-1}) and 123°C (6.0 kJ mol^{-1}), using the asymmetric double Gaussian cumulative function in Peakfit® 4.0. On the

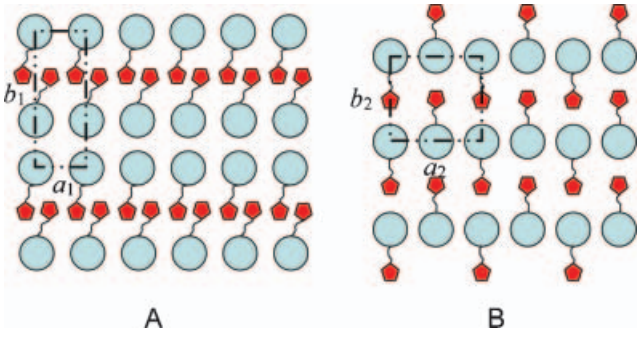

Figure 5. Schematics of two highly ordered Col_r structures in **2c**. (A) A bilayer Col_r structure (plane group *pm*), (B) a single-layer Col_r structure (plane group *p2mg*). The 2D unit cells are also shown.

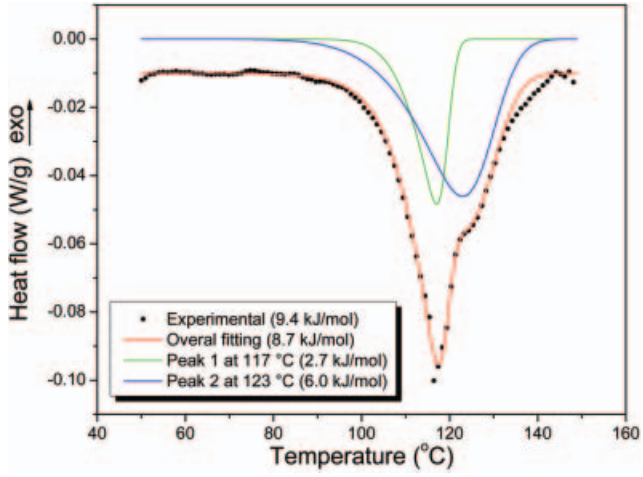

Figure 6. DSC first heating curve for **2c**. The isotropization peak is deconvoluted into two peaks at 117 and 123°C. The regression coefficient of the curve fitting is 0.9932.

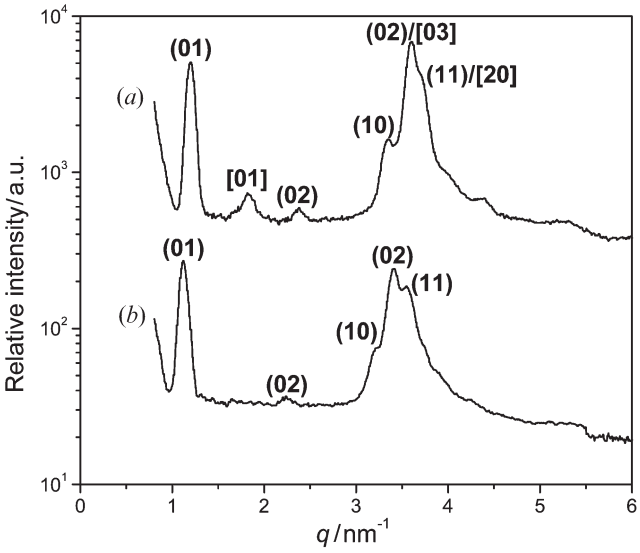

Figure 7. 1D low angle XRD profiles for (*a*) original **2c** and (*b*) **2c** annealed at 95°C for 60 h. The Miller indices in parenthesis and brackets are for models A and B in figure 4, respectively.

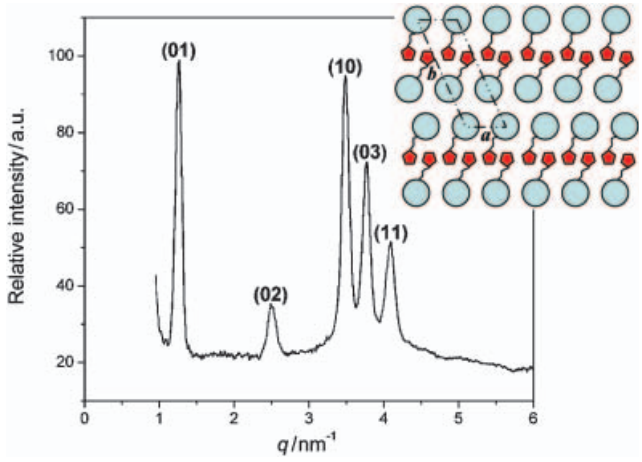

Figure 8. 1D SAXS profile for **2b** with assigned Miller indices. The inset shows a schematic of the Col_o phase.

basis of XRD results, the bilayer Col_r phase is a major component. Therefore, the T_I values for the single-layer and bilayer Col_r phases could be assigned as 117 and 123°C, respectively. Both the T_I and heat of transition appeared higher for the first heating than in subsequent runs. This might be because the original sample had higher liquid crystallinity as it was cast from THF.

Compared with the bilayer Col_r structure, the single-layer Col_r phase was metastable. Annealing at elevated temperature (95°C) for 60 h eliminated the single-layer Col_r structure in the sample. The DSC result for the annealed sample showed only a single isotropization peak during heating, similar to that in figure 2(*d*). The one-dimensional (1D) XRD results are shown in figure 7; the [0 1] reflections from the single-layer Col_r phase disappeared after annealing. This might be because the imidazolium layer density in the single-layer Col_r phase was lower than that in the bilayer Col_r phase (see figure 5). The single-layer Col_r, therefore, was a kinetically formed structure. The columnar unit cell dimensions enlarged slightly after annealing at high temperatures: $a=5.62$ nm, $b=1.96$ nm, and thus the density decreased to $\rho=0.87\,g\,cm^{-3}$.

The structure of **2b** was determined by X-ray experiments. Figure 8 shows 1D SAXS curve of **2b** with assigned Miller indices on the basis of an oblique cell: $a=1.90$ nm, $b=5.29$ nm, $\alpha=109°$. Different from the structure of **2c**, no single-layer Col_r phase was observed in **2b**. The oblique columnar (Col_o) phase was further supported by 2D X-ray results on shear-oriented **2b** samples. The 2D SAXS and WAXD patterns are shown in figure 9. In the 2D SAXS pattern (figure 9A), the observation of a split 'X' pattern for the (10) reflection indicated that the *a*-axis was inclined to the *b*-axis. The (1 1) reflections were also seen in the quadrant. In the 2D WAXD pattern (figure 9B), the intra-column (or inter-disk) spacing was seen at 0.36 nm. Since this reflection (0.36 nm) was orthogonal to the (0 3) (or layer) reflection, it was concluded that the normal of the triphenylene disk was oriented parallel to the column axes.

The lamellar structure in **2c** was visualized by TEM (see figure 10). The sample was cryo-microtomed at −20°C to obtain ~75–100 nm thin sections using a diamond knife, followed by staining with I_2 vapor [10]. The dark layers appeared thinner than the bright layers, which suggested that I_2 preferentially stained the imidazolium salt moieties in the triphenylene molecules. Since **1c** did not exhibit any liquid crystalline behaviour, while **2c** showed columnar phases after quaternization, we conclude that it was the ionic interactions that induced the microphase separation and thus lamellar packing of the imidazolium salts.

4. Conclusions

We have observed highly ordered columnar mesophases in asymmetric imidazolium triphenylene salts, **2b** and **2c**. Ionic interactions among asymmetric imidazolium salts in the triphenylenes, rather than their molecular (discotic) shapes, induced novel columnar supramolecular self-assembly with layer structures. The lower limit of the liquid crystalline ranges extended to −10°C for **2b** and −20°C for **2c**. This may enable them to serve as potential candidates for novel ionic materials in LC devices and ion transport membranes.

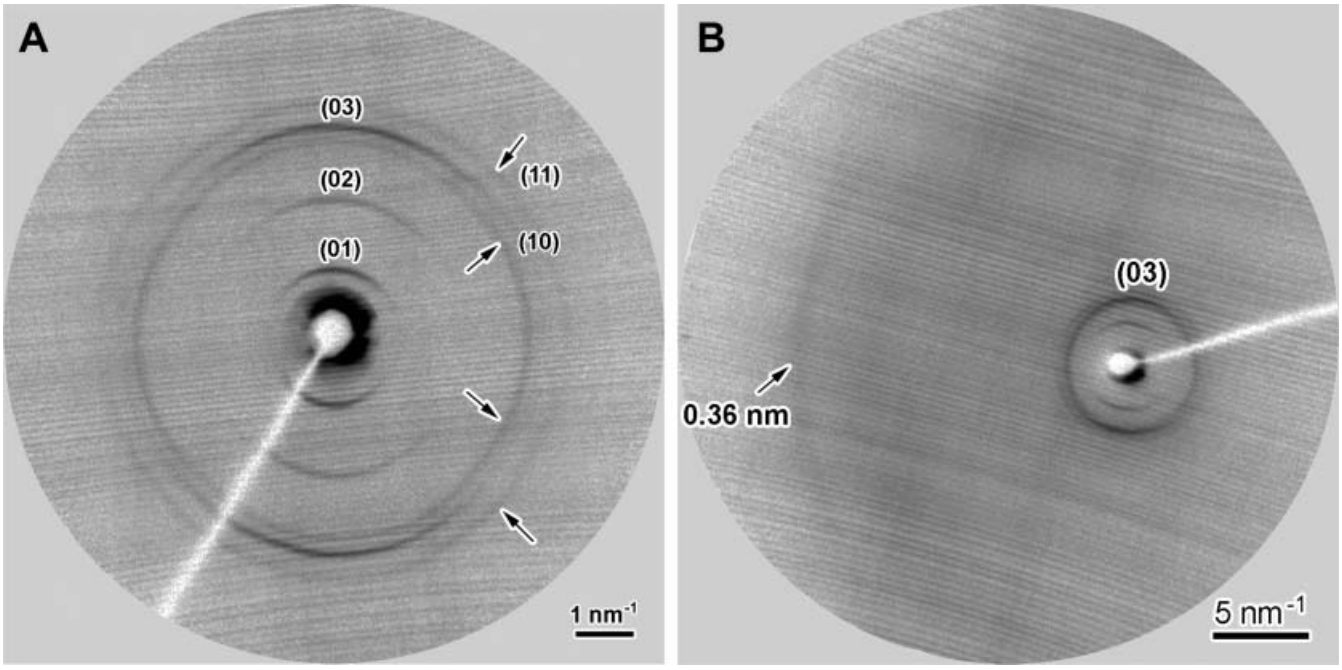

Figure 9. (A) 2D SAXS and (B) 2D WAXD patterns for **2b** with assigned Miller indices. Intensities in both patterns are in logarithmic scales.

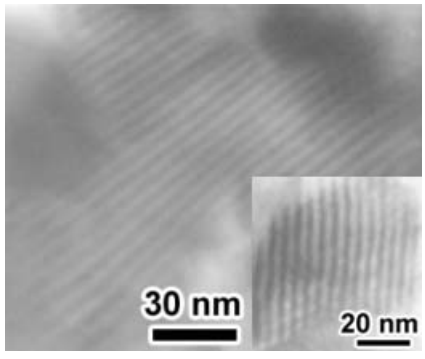

Figure 10. Bright field TEM micrographs of **2c** thin sections stained by I_2 vapour.

Acknowledgements

This work was supported by NSF CAREER award DMR-0348724, DuPont Young Professor Grant, and 3M Nontenured Faculty Award.

References

[1] (*a*) M. O'Neill, S.M. Kelly. *Adv. Mater.*, **15**, 1135 (2003); (*b*) C.D. Simpson, J. Wu, M.D. Watson, K. Müllen. *J. mater. Chem.*, **14**, 494 (2004).

[2] (*a*) A.M. van de Craats, J.M. Warman, A. Fechtenkotter, J.D. Brand, M.A. Harbison, K. Müllen. *Adv. Mater.*, **11**, 1469 (1999); (*b*) A.M. van de Craats, J.M. Warman. *Adv. Mater.*, **13**, 130 (2001); (*c*) M. Lee, J.-W. Kim, S. Peleshanko, K. Larson, Y.-S. Yoo, D. Vaknin, S. Markutsya, V.V. Tsukruk. *J. Am. chem. Soc.*, **124**, 9121 (2002).

[3] (*a*) S. Kumar, D.S.S. Rao, S.K. Prasad. *J. mater. Chem.*, **9**, 2751 (1999); (*b*) R.J. Bushby, N. Boden, C.A. Kilner, O.R. Lozman, Z. Lu, Q. Liu, M.A. Thornton-Pett. *J. mater. Chem.*, **13**, 470 (2003); (*c*) J. Motoyanagi, T. Fukushima, T. Aida. *Chem. Commun.*, 101 (2005).

[4] (*a*) P.H.J. Kouwer, G.H. Mehl. *Angew. Chem. int. Ed.*, **42**, 6015 (2003); (*b*) P.H.J. Kouwer, J. Pourzand, G.H. Mehl. *Chem. Commun.*, 66 (2004).

[5] (*a*) K. Ohta, H. Muroki, A. Takagi, K. Hatada, H. Ema, I. Yamamoto, K. Matsuzaki. *Mol. Cryst. liq. Cryst.*, **140**, 131 (1986); (*b*) D. Janietz, R. Festag, C. Schmidt, J.H. Wendorff. *Liq. Cryst.*, **20**, 459 (1996).

[6] S. Kumar, S.K. Pal. *Tetrahedron Lett.*, **46**, 4127 (2005).

[7] (*a*) J.A. Schröter, C. Tschierske, M. Wittenberg, J.H. Wendorff. *J. Am. chem. Soc.*, **120**, 10669 (1998); (*b*) S.A. Ponomarenko, N.I. Boiko, V.P. Shibaev, R.M. Richardson, I.J. Whitehouse, E.A. Rebrov, A.M. Muzafarov. *Macromolecules*, **33**, 5549 (2000); (*c*) T. Komatsu, K. Ohta, T. Watanabe, H. Ikemoto, T. Fujimoto, I. Yamamoto. *J. mater. Chem.*, **4**, 537 (1994); (*d*) V. Percec, M. Glodde, T.K. Bera, Y. Miura, I. Shiyanovskaya, K.D. Singer, V.S.K. Balagurusamy, P.A. Heiney, I. Schnell, A. Rapp, H.-W. Spiess, S.D. Hudson, H. Duan. *Nature*, **419**, 384 (2002); (*e*) D. Goldmann, D. Janietz, C. Schmidt, J.H. Wendorff. *J. mater. Chem.*, **14**, 1521 (2004).

[8] L. Cui, J. Miao, L. Zhu. *Macromolecules*, **39**, 2536 (2006).

[9] (*a*) M.T. Allen, S. Diele, K.D.M. Harris, T. Hegmann, B.M. Kariuki, D. Lose, J.A. Preece, C. Tschierske. *J. mater. Chem.*, **11**, 301 (2001); (*b*) N. Boden, R.C. Borner, R.J. Bushby, A.N. Cammidge, M.V. Jesudason. *Liq. Cryst*., **15**, 851 (1993); (*c*) S. Kumar, M. Manickam. *Synthesis*, 1119 (1998).

[10] J. Washiyama, C. Creton, E.J. Kramer. *Macromolecules*, **25**, 4751 (1992).

[11] I. Paraschiv, P. Delforterie, M. Giesbers, M.A. Posthumus, A.T.M. Marcelis, H. Zuilhof, E.J.R. Sudhölter. *Liq. Cryst.*, **32**, 977 (2005).

[12] T. Hahn (Eds). *International Tables for Crystallography*. Kluwer Academic Publishers, Dordrecht (1995). Vol. A.

[13] S. Chandrasekhar, G.S. Ranganath. *Rep. Prog. Phys.*, **53**, 57 (1990).